10-22-2021

CD44-targeted, indocyanine green-paclitaxel-loaded human serum albumin nanoparticles for potential image-guided drug delivery.

Karthik Thangavel
Thomas Jefferson University

Asha Lakshmikuttyamma
Thomas Jefferson University

Chellappagounder Thangavel
Thomas Jefferson University

Sunday A. Shoyele
Thomas Jefferson University

CD44-Targeted, Indocyanine green-Paclitaxel-Loaded Human Serum Albumin Nanoparticles for Potential Image-Guided Drug Delivery

Karthik Thangavel[1], Asha Lakshmikuttyamma[1], Chellappagounder Thangavel, Sunday A. Shoyele[1*]

[1]Department of Pharmaceutical Science, Jefferson College of Pharmacy, Thomas Jefferson University

[2]Department of Dermatology, Jefferson College of Pharmacy, Thomas Jefferson University

***Corresponding Author:**

Dr. Sunday A Shoyele

Associate of Pharmaceutical Sciences

College of Pharmacy

Thomas Jefferson University

9th Floor. 901 Walnut Street

Philadelphia. 19107

USA

Tel: 215-503-3407

Email: Sunday.Shoyele@jefferson.edu

Abstract

The use of multifunctional nanomedicines for image-guided drug delivery is currently being universally evaluated as a means of efficiently managing cancers and other diseases. In this study we evaluated the potential of an indocyanine green (ICG) and paclitaxel (PTX) loaded human serum albumin (HSA) nanoparticles that was conjugated with hyaluronic acid for use in image-guided drug delivery targeted to CD44-positive non-small cell lung cancer (NSCLC). Series of NSCLC cell lines were evaluated for the expression of CD44 using both western blot analysis and qRT-PCR and compared to a normal lung fibroblast cell line (MRC-5). Using Fluorescence microscopy and photoacoustic imaging (PA), we explored the ability of these targeted nanoparticles to selectively accumulate in NSCLC cell lines in comparison to MRC-5 and their potential for biomedical imaging towards their use for theranostic application. Results obtained suggest that these targeted nanoparticles have potential for application in both imaging and treatment of NSCLC.

Introduction

The advent of multifunctional nanomedicine is currently generating widespread attention for targeted specialized nanoparticles, mainly because of the ability of these nanoparticles to potentially be used for simultaneous diagnosis and treatment of various diseases. The use of these multifunctional nanomedicines for image-guided drug delivery is currently being universally evaluated as a means of efficiently managing cancers and other diseases [1-3]. Nevertheless, clinical application of nanoparticles for disease detection and therapy has been limited by off-target effects and poor cellular uptake. For maximum application in cancer detection and therapy, it is important that nanoparticles are able to target tumor with limited accumulation in healthy normal tissues. Human serum albumin (HSA) as a drug carrier is one of the most elegant and promising ways to exploit the so-called enhanced permeability and retention effect (EPR) which is an essential "passive targeting" strategy for cancers [4]. Abraxane®, an albumin-bound nanoparticle formulation of paclitaxel, currently approved for non-small cell lung cancer (NSCLC), as well as aldoxorubicin, which is currently in phase III studies are two examples [5, 6]. However, albumin as a passive targeting carrier is often not precise enough especially when the carrier has an additional function of cancer detection. In view of this, an active targeting component is needed to increase the targeting efficiency of these nanoparticles. In this study, we conjugated hyaluronic acid (HA) via EDC/NHS bonding to HSA to produce a nanoparticle delivery system that will precisely deliver indocyanine green (ICG), for tumor detection and paclitaxel (PTX), a chemotherapeutic agent, precisely to lung tumor to detect, monitor and simultaneously treat NSCLC. HA is a ligand that specifically binds to CD44. Standard and variant CD44 isoforms are commonly expressed in lung cancer of the non-small cell type but not the small cell type [7]. HA is a naturally occurring polysaccharide present in the extracellular matrix and synovial fluids. Its biocompatibility and biodegradability has made it a popular choice for biomedical applications such as tissue engineering, drug delivery and molecular imaging. Further, HA nanoparticles have been demonstrated to more efficiently accumulate in tumor site than pure water-soluble HA when systemically administered into mice [8].

Morever, both Abraxane® and aldoxorubicin are based on passive targeting strategy, which is not always as precise as needed, especially when there is also a need for precise detection and monitoring of tumor. To effectively control the growth of NSCLC, an innovative modality, which can simultaneously detect and treat this highly debilitating disease, at an early stage is highly essential. To achieve this, our team are in the process of developing a nanoparticle delivery system composing of a covalently bonded human serum albumin (HSA) and hyaluronic acid (HA), two highly safe and approved materials. These nanoparticles are then loaded with PTX (a first line chemotherapeutic agent for NSCLC) and ICG which is a water soluble tricarbocyanine dye. Along with methylene green, it is the only dye, clinically approved near infrared red fluorophore to form HA-functionalized ICG-PTX loaded nanoparticles . It has been approved by the FDA for human imaging and diagnosis in clinical applications. It is often used as a contrast agent for photoacoustic imaging (PA).

PA imaging is a technique that combines high spatial resolution of ultrasound (US) and high contrast of optical imaging systems. PA imaging enables the gathering of functional and molecular information in real time and works at clinically relevant imaging depth [9-10]. PA imaging of nanoparticle-encapsulated contrast agents for disease diagnosis is an emerging field of biomedical imaging. PA imaging is currently being studied for imaging in small vertebrates and currently not being used in humans as the depth of its sensitivity is not applicable to human yet. However, techniques such as ultrasound imaging can also be used for image-guided drug delivery.

This study investigates the potential theranostic application of a nanoparticle delivery system composed of covalently bound HSA-HA combination for efficient targeting of NSCLC tumor to enable both detection by PA and treatment.

Material and methods

Chemicals and solvents

Hyaluronic acid (low molecular weight, 4660 Da) was obtained from R and D Systems, Inc. (Minneapolis, MN). Albumin from human serum (Lyophilized ≥ 96%) was obtained from Sigma Aldrich (St. Louis, MO). Fluorescein isothiocyanate (FITC), 4′,6-diamidino-2-phenylindole (DAPI), potassium phosphate monobasic, potassium hydroxide, sodium phosphate dibasic, sodium phosphate monobasic, acetic acid (99.8%) and acetonitrile were obtained from ThermoFisher Scientific (Waltham, MA). Ethyl alcohol, anhydrous was purchased form Decon Laboratories (King of Prussia, PA). Indocyanine green was obtained from MP Biomedicals LLC (Salon, OH). Paclitaxel was purchased from LC Laboratorie (Woburn, MA).

Cell Culture

NSCLC cell lines (H1299, A549, H460 and H23) and normal lung fibroblast cell line (MRC-5) were purchased from American Type Culture Collection, ATCC (Manassas, VA) and were cultured in appropriate culture media. H1299, H460 and H23 cells were cultured in RPMI 1640, A549 cells were cultured in F12K and MRC-5 was maintained in Eagle's Minimum Essential Medium. These media were supplemented with 10% fetal bovine serum (FBS) and 1% of penicillin/streptomycin. The cells were incubated in a humidified 5% carbon-dioxide and 95% air incubator at 37°C.

Preparation of HA-functionalized ICG-PTX loaded nanoparticles.

5 mg/ml of HSA was dissolved in 10 ml of double-distilled deionized water before adding 2 mg of ICG with gentle mixing on a magnetic stirrer. 15 ml of dehydrated ethanol was slowly added to the mixture, forming a ratio of water:ethanol, 1:1.5. For nanoparticles containing PTX, 50 mg of PTX was dissolved in the 15 ml of dehydrated alcohol before gently adding it to the HSA solution. Formed nanoparticles are continuously stirred on the magnetic stirrer for 10 minutes. Nanoparticle mixture is then aliquoted into 5 ml-Eppendorf tubes and centrifuged at 10000 rpm for 5 minutes. The supernatant was decanted and used for analysis of unencapsulated ICG and PTX by HPLC-UV.

As a control experiment, we performed the process without HSA in the distilled water but the PTX dissolved in the dehydrated alcohol. No precipitate was seen possibly because the ratio of water:alcohol was not enough to precipitate the PTX on its own.

FITC-loaded nanoparticles were prepared in a similar way by replacing the ICG with 2 mg FITC. Every other sequence was kept consistent.

The amount of unecapsulated ICG and PTX determined by HPLC-UV was used to calculate the loading capacity (LC) and encapsulation efficiency (EE) of these payloads, using the following equation [11, 12]:

$$LC = \frac{\text{Amount of drug used} - \text{amount of drug unencapsulated}}{\text{Total weight of nanoparticles produced}} \times 100$$

And:

$$EE = \frac{\text{Amount of drug used} - \text{amount of drug unencapsulated}}{\text{Amount of drug used}} \times 100$$

It is also important to state that the nanoparticles were thoroughly washed to remove any adsorbed ICG and PTX on the nanoparticles to ensure we do not have false EE results.

To conjugate HA to the nanoparticles, 1-ethyl-3-(3-dimethylaminopropyl) carbodiimide hydrochloride (EDC) and N-hydroxysulfosuccinimide (NHS) were used to activate the carboxyl group in the HSA nanoparticles and act as a crosslinker between the carbonyl group of the HSA and the amino group present in HA. This was done by dispersing 10 mg of the preformed nanoparticles in 10 ml of citrate buffer. 40 mM of EDC and 10 mM of NHS were added and stirred for 15 minutes at room temperature. 1 ml of 5 mg/ml of HA was added and mixed at

room temperature for 2 hr. This was then centrifuged in 10 kDA dialysis tube at 4000 rpm to get rid of the unattached HA.

Lyophilization of nanoparticles
Prepared nanoparticles were rinsed with double-distilled deionized water following centrifugation in Eppendorf tubes before being redispersed in water. This was then snap-frozen using liquid nitrogen. Frozen nanoparticles were loaded into a freeze dryer (Labconco FreezeZone 4.6), and lyophilization was performed for 48 hr.

Fourier transform-infrared spectroscopy
Lyophilized nanoparticles were sampled on the surface of a iS10 FT-IR spectrometer (Thermo Fisher Scientific) installed with a single-reflection attenuated total reflectance (ATR) with a diamond internal reflection crystal. Using a 4 cm^{-1}, spectra were collected for each sample after 64 scans before analyzing the data using OMNIC software.

Nanoparticle characterization
The size of the different batches of nanoparticles prepared was measured immediately after production and repeated after storage at room temperature after 7 days to see if any agglomeration might occur, using photon correlation spectroscopy. Each sample was sonicated in a water bath for approximately 3 minutes before pouring aliquot into disposable cuvette. Using ZetaSizer Nano ZS (Malvern Instruments, Malvern, UK), Intensity autocorrelation was measured at a scattering angle (θ) of 173°. The Z-average and polydispersity index (PDI) were recorded in five independent measurements. The zeta potential (ζ) for each batch of nanoparticle was measured by pouring aliquot of samples dispersed in double distilled deionized water into a universal dip cell (Malvern Instruments, Malvern, UK) and the ζ recorded in five independent measurements.
The morphology of prepared nanoparticles was confirmed using scanning electron microscopy (SEM). Water dispersed samples were dropped on the surface of a double-sided carbon disc and left to dry at room temperature. Dried samples were then palladium coated on an aluminum stub before being mounted on a Zeiss Supra 50 V system (Carl Zeiss Meditec AG, Jena, Germany and relevant images were recorded.

Drug release studies
The release of both ICG and PTX from the HA-functionalized ICG-PTX loaded nanoparticles was monitored at pH values 6.6 and 7.4. 10 mg of nanoparticles was weighed and dispersed into 0.50 ml of the buffer solution. This was then transferred into a tubular cellulose dialysis membrane secured at both ends to prevent leakage. The dialysis tube was placed in a beaker containing 7 ml of the buffer solution before being stored in an incubator maintained at 37°C. At predetermined time points 500 µL of the buffer solution was sampled and stored in the refrigerator until analysis by HPLC.

Size exclusion-HPLC (SE-HPLC)
HA was quantitatively analyzed using SE-HPLC [13]. HA samples were run using an isocratic mobile phase of 0.05 M potassium dihydrogen sulphate, pH 7 (pH adjustment was done using 10% potassium hydroxide). Samples were run thorough a BioSep SEC S2000, 300 mm x 7.8 mm analytical column installed in a Waters 2695 separation module combined with a Waters 2998 photodiode array detector Alliance HPLC system (Waters, Milford, MA, USA). Samples were run at a constant flow rate of 0.5 mL/min with the detector set at 205 nm. The volume of sample injected was 10 µL.

HPLC analysis

The concentrations of ICG and PTX contained in / released from the HA-functionalized ICG-PTX loaded nanoparticles were determined by HPLC-UV analysis. The instrument of choice was a Waters 2695 separation module combined with a Waters 2998 photodiode array detector Alliance HPLC system (Waters, Milford, MA, USA). To measure ICG, chromatographic separation was performed using a Clarity Oligo-RP column (3µm, 50x2.0 mm; Phenomenex, Torrance, CA, USA) at 20°C. Using an injection volume of 10 µL, an isocratic mobile phase of acetonitrile and 0.1M acetate buffer pH 3 (45:55,v/v) was pumped at a flow rate of 0.5 mL/min. Eluents were measured at 225 nm.

To measure PTX, chromatographic separation was carried out using a Clarity Oligo-RP column (3µm, 50×2.0 mm; Phenomenex, Torrance, CA, USA) at 20°C). Using an injection volume of 10 µL, gradient elution using both water and acetonitile was adopted from Badea et al. [14]. 40% acetonitrile was run from 0 to 18 minutes: 45% acetonitrile was run from 18 to 20 min and 100% acetonitrile was run for 20–35 min. The flowrate was 0.5 mL/min and injection volume was 10 µL. The detection was at 227 nm.

MTT assay

1×10^4 cells were seeded per well in 96-well plates. These cells were incubated for 24 hours at 37°C in a humidified atmosphere with 5% carbon dioxide. They were then treated with different concentrations of various nanoparticle formulation in Opti-MEM for 6 hours. Cells were then washed with PBS X3 before the media was replaced with fully supplemented RPMI medium. Following 72 hour incubation, cells wer treated with 10 µL of 12 mmol/L MTT reagent and incubated for 4 hours at 37°C. 50 µL of sterile dimethyl sulfoxide was added after the medium was aspirated. The cells were then incubated at 37°C for 10 minutes. The plate was read at 540 nm and 650 nm.

Fluorescence microscopy

Cells at a density of $2 \text{ X } 10^4$ were seeded in eight-well coated glass slides obtained from Discovery Labware, (Tewksbury, MA, USA). After 48 hour incubation, they were washed with PBS and incubated with different nanoparticle formulations dispersed in the Opti-Mem medium at a concentration of 100 µg/mL for 6 hours. PBS washed cells were then fixed using 2% paraformaldehyde, and incubated at room temperature for 20 minutes. 5% BSA was added to the cells for 30 minutes at room temperature. Cells were stained with AlexaFluoro-555-labeled wheat germ agglutinin (WGA-AF-555) before being stained with DAPI to visualize nucleus. Cells were then observed under Leica DMI 6000B fluorescence microscope (Leica Microsystems, Wetzlar, Germany).

Flow cytometry

Cells ($1 \text{ x } 10^6$) were seeded in petri-dish and incubated for 48 hours. Using nanoparticles HA-functionalized FITC-PTX loaded nanoparticles, cells were treated with 100 µg/mL nanoparticles dispersed in Opti-MEM medium. The cells were then incubated for 6 hours. Another group of cells were pretreated with ten times excess of free HA, approximately 60 minutes before being treated with HA-functionalized FITC-PTX loaded nanoparticles. After decanting the Opti-MEM medium, cells were washed with PBS three times. After trypsinization, ell were centrifuged and the pellet was washed and resuspended in PBS. Before being analyzed by flow cytometry (BDFACS caliber), a 0.75 µm cell strainer was used to filter the cells to prevent cell aggregates from blocking the tube lines of the instrument.

Photoacoustic imaging (PA imaging)

To prepare HA-functionalized ICG-PTX loaded nanoparticles for application as a contrast agent in vivo, we tested these nanoparticles in biological phantoms. Using a polymeric blood vessel-

mimicking tubes in a water bath, we evaluated the ability of these nanoparticles to enhance the signal sensitivity of ICG as compared to free ICG. Images were captured by PA Vevo® LAZR system (FujiFilm VisualSonics, Amsterdam, Netherlands) at approximately 800 nm. Maximum PA intensities were obtained after laser irradiation at 806 nm. To detect the signal of HA-functionalized-ICG-loaded nanoparticles at various depths, a chicken muscle phantom was used to mimic a tissue environment before imaging. This was done to ensure that PA imaging using ICG as a contrast agent could be applicable to orthotopic NSCLC mice models. Samples were injected at depths, 2, 5 and 10 mm into the chicken muscles.

Quantitative Reverse Transcription (RT) PCR analysis
Total RNA was isolated using Qiagen RNAeasy kit (Qiagen, Valencia, CA). Equal amount of RNA from different lung cancer cell lines were reverse transcribed using Verzo cDNA kit (Thermoscientific Waltham, MA). Quantitative PCR of CD44 was carried out using TaqMan gene expression assay method (Life technologies, Waltham, MA). GAPDH expression was used to normalize CD44 expression levels.

Results

Nanoparticle characterization
HA-functionalized ICG-PTX loaded nanoparticles were prepared by a desolvation process by dropwise addition of dehydrated ethanol to an aqueous solution of HSA. Before settling on a ratio of 1: 1.5 ratio of water:ethanol, we tried different ratios before settling for 1:1.5 due to the superior yield. SEM micrographs in Figure 1 confirms that the nanoparticles are spherical in shape. Figure 1A demonstrates that the non-functionalized nanoparticles were discrete in nature while Figure 1B, demonstrates that the process of functionalization with HA lead to more agglomerated nanoparticles probably because of the sticky nature of HA polymer and the multiple steps involved in the conjugation process.
Particle size analysis by photon correlation spectroscopy presented in Table 1. This demonstrates that the empty nanoparticles had the lowest particle size of 202 nm. Both PTX-loaded nanoparticles and ICG-loaded nanoparticles have smaller sizes as compared to the ICG-PTX-loaded nanoparticles. This is quite expected as the inclusion of both payloads lead to an increase in the size of the particles. Conjugation of HA to ICG-PTX-loaded nanoparticles increase the size of the nanoparticles from 242.56 nm to 315.24 nm. Further, there was no significant change in particle size after 7 days of storage at room temperature, demonstrating the stability of these nanoparticles. The polydispersity index (PDI) in Table 1, further demonstrate the slight differences in these different nanoparticle formulations and confirms that they are mostly monodispersed as corroborated by the PDI of all the formulation being less than 0.3.
The zeta potential (net charge) for all the nanoparticles were mostly negative at approximately –7 mV. The conjugation of HA to the ICG-PTX-loaded-HSA-nanoparticles led to more negatively charged nanoparticles as shown in Table 1.

Table 1. Particle size and Zeta potential of different HSA nanoparticles. Results are presented as the mean of five independent measurements. (Mean, n = 5), STDDev was collected from the Malvern DLS software.

Nanoparticles	Size (nm) 0 days after production	STDDev 0 days after production	PDI	Size (nm) 7 days after production	STDDev 7 days after production	Zeta potential (ζ) mV
Empty nanoparticles	202	11.2	0.116 ± .060	201	12.1	- 7.62 ± 0.54
PTX-loaded nanoparticles	207	12.3	0.105 ± 0.015	209	13.2	- 7.22 ± 0.44
ICG-loaded nanoparticles	220	10.4	0.165 ± 0.168	220	11.4	- 7.33 ± 3.45
ICG-PTX-loaded nanoparticles	243	13.4	0.160 ± 0.162	240	12.4	- 6.58 ± 0.75
HA-functionalized ICG-PTX loaded nanoparticles	315	24.3	0.256 ± 0.065	316	24.3	-9.56 ± 0.65

Table 2, shows that the EE of PTX in the PTX-loaded nanoparticles was not significantly different from that of ICG-PTX-loaded nanoparticles (P≥0.001), suggesting that the presence of ICG did not adversely affect the encapsulation of PTX. Similarly, the LC of PTX in the PTX-loaded nanoparticles was not significantly affected by the presence of ICG (P≥0.001). For ICG, although the EE of both ICG-loaded nanoparticles and that of ICG-PTX nanoparticles are very similar, the LC of ICG in ICG-PTX-loaded nanoparticles is approximately half of that of ICG-loaded nanoparticles.

Table 2. Loading capacity (LC) and Encapsulation efficiency (EE) of the payloads in the various HSA-based nanoparticles. Results are presented as Mean±SD of five independent measurements.

Nanoparticles	LC for PTX (%) Mean±SD (n=5)	EE for PTX (%) Mean±SD (n=5)	LC for ICG (%) Mean±SD (n=5)	EE for ICG (%) Mean±SD (n=5)
Empty nanoparticles	0	0	0	0
PTX-loaded nanoparticles	65.3 ± 2.7	81.2 ± 3.4	-	-
ICG-loaded nanoparticles	-	-	4.44 ± 0.31	69.0 ± 2.1
ICG-PTX-loaded nanoparticles	70.8 ± 0.7	88.5± 1.2	2.23 ± 0.42	69.25 ± 3.3

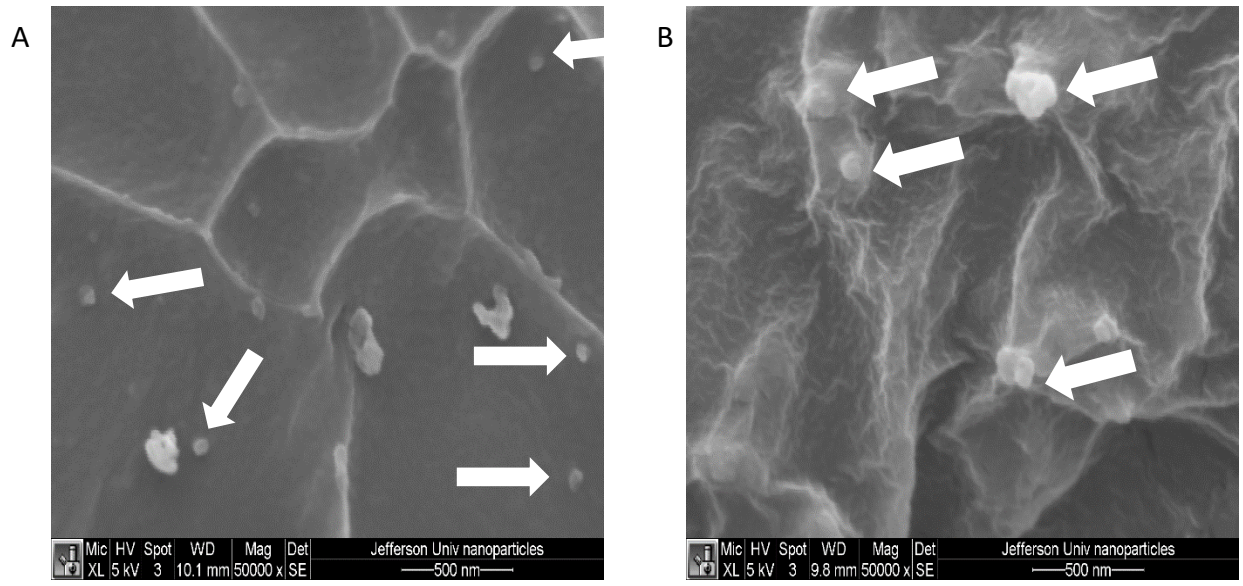

Figure 1. Nanoparticle characterization. A. SEM image of non-functionalized ICG-PTX-loaded nanoparticles B, SEM micrograph showing the nanoparticles after conjugation of HA to form HA-functionalized ICG-PTX-loaded nanoparticles. The later appear more agglomerated because of the many steps involved in the conjugation process. The white arrows point to the nanoparticles.

Release of ICG and PTX from nanoparticles

The release of both ICG and PTX from HA-functionalized ICG-PTX-loaded nanoparticles was monitored at pH values 7.4 and 6.6 to represent the pH values of the blood and tumor microenvironment, respectively [15]. Figure 2A shows that PTX demonstrated a more efficient release from the nanoparticles at pH 6.6 with approximately 100% of the drug released after 46 hr while only approximately 30% of PTX was released at pH 7.2. This suggests that the loaded PTX will not be released at pH close to the pH of circulating blood but rather at a pH close to that of the tumor microenvironment. The reason for the more efficient release at pH 6.6 could be attributed to the acidic nature of the tumor microenvironment which facilitates the graduate erosion of the HSA-nanoparticles, hence enabling a slow but controlled release of the loaded PTX. To verify this, we took samples for measurement at 5 and 10 hr during the release studies. At 5 hr the size of the nanoparticles decreased from the initial 315 nm to approximately 301 nm which further reduced to approximately 292 nm after 10 hr.

It is however, important to know that the plasma, and sink conditions present in vivo would most likely accelerate the release of both PTX and ICG.

Similar trend was observed for ICG in Figure 2B. However, ICG was released faster from the nanoparticles possibly because of its superior solubility in aqueous medium when compared to PTX, hence 100% loaded ICG was already release after 2 hr at pH 6.6 while only approximately 50% was released at pH 7.2.

We performed a control in which we used free PTX/ICG. The drugs were quickly on the other side of the membrane within a seconds showing what we had prior was a release and not permeation.

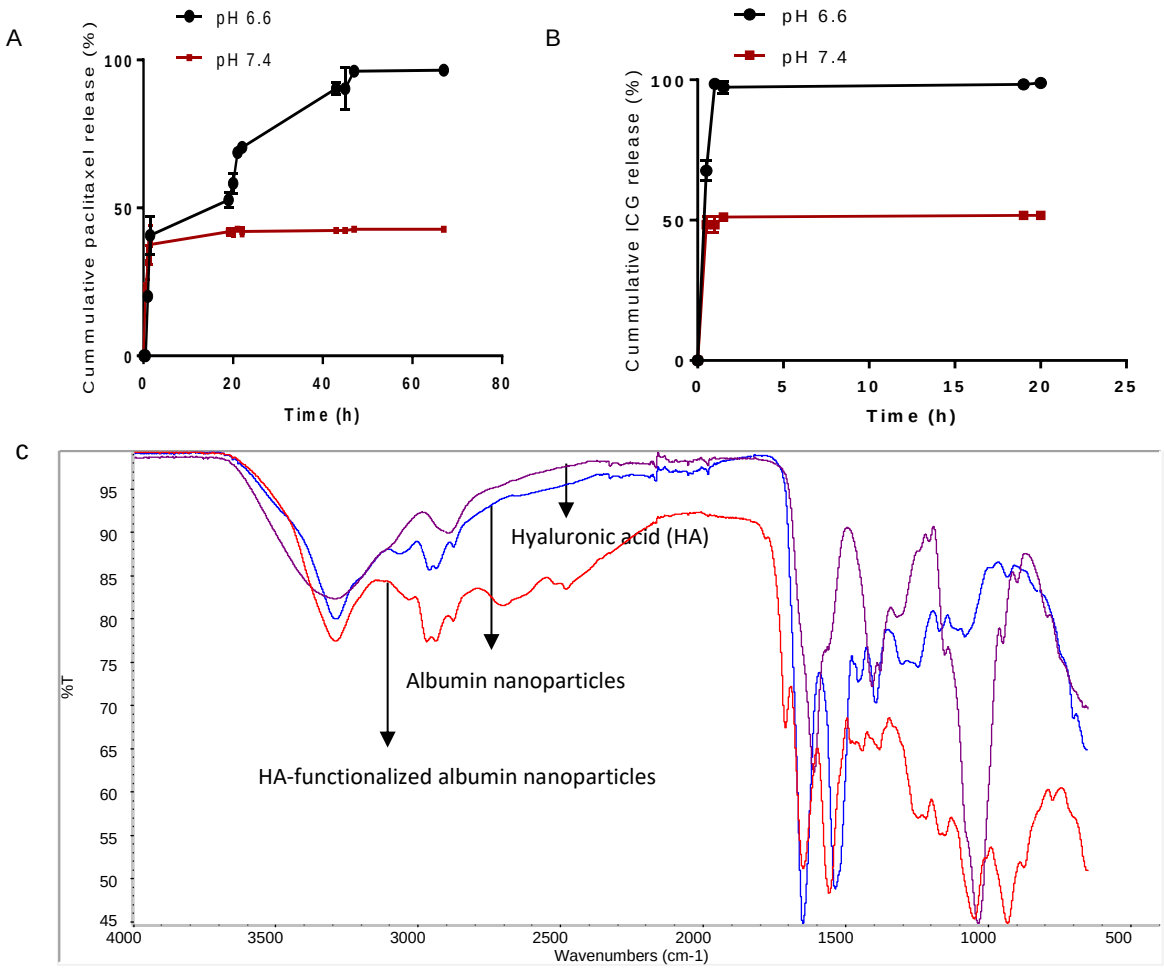

Figure 2. Drug Release profile. Release of PTX and ICG was monitored by collecting aliquot amount (500µl) from the reservoir of citrate buffer pH 6.6 and PBS pH 7.4 and analyzing the cumulative amount of drug release over time using HPLC. A, represents the release profile of PTX while B, represents the release profile of ICG over a sustained period of time. C. FITR spectra verifying the covalent conjugation of HA to albumin-based nanoparticles.

Confirmation of Conjugation of HA to nanoparticles by FTIR

Conjugation of HA to the HSA-nanoparticles was verified by FT-IR spectroscopy. Figure 2C shows the differences in the spectrum of HA-functionalized-HSA-nanoparticles when compared to the non-functionalized-HSA-nanoparticles and the unconjugated HA. The reaction between amino group (NH_2) of HA and the carboxylic group (COOH) of HSA is the driving force between the conjugation of these two molecules.The non-functionalized-HSA-nanoparticles spectrum exhibits a band at approximately 3284 cm^{-1}. This band is attributable to the group stretching vibration of both NH_2 and OH amide group from the amino acid residues of HSA. Similarly, a band is reported at approximately 3290 nm in the HA spectrum. This is also attributable to the amide group present in the HA [16, 17]. In contrast, this band became more prominent with a slight shift to 3285 cm^{-1} in the spectrum of HA-functionalized-HSA-nanoparticles suggesting the presence of an interaction between both the non- functionalized-HSA-nanoparticles and the unconjugated HA due to their conjugation and the presence of additional amide bonds. The presence of a new amide bond was also observed at 1645 cm^{-1} in the spectrum of the HA-

functionalized-HSA-nanoparticles. A similar band observed at 1647 cm^{-1} is due to the amide II carbonyl stretch from the HSA (protein). However, there is a slight shift to a higher band at 1708 nm in the HA-functionalized-HSA-nanoparticles, due to formation of new amide II bonds. Further, the band that was observed at approximately 1031 cm^{-1} in the HA spectrum but absent in the non-functionalized HSA-nanoparticle, can be clearly observed at 1046 cm^{-1} in the HA-functionalized-HSA-nanoparticles spectrum. This band is attributable to the stretching from the secondary alcohol in the HA [18]. The slight change in position is due to the conjugation of HA to the nanoparticles.

Cellular uptake of nanoparticles

To confirm the influence of CD44 on selective uptake of HA-functionalized-ICG-PTX-loaded nanoparticles, both western blot and qRT-PCR analysis to measure and compare the expression of CD44 in four NSCLC cells, H1299, A549, H23 and H460, and one normal lung fibroblast cell, MRC-5. As seen in the western blot analysis in Figure 3A, normal lung fibroblast cell MRC-5 did not express any CD44 while the NSCLC cells showed different levels of CD44 expression. qRT-PCR was then used to quantify and compare the levels of CD44 expression in the NSCLC cells. Figure 3B, demonstrates that the highest level of CD44 expression was in H1299, followed by A549 with both H23 and H40 with relatively lower level of expressions. Consequence to this, we decided to move ahead with both H1299 and A549 and compare their uptake of the nanoparticles to that of the CD44-negative MRC-5. To monitor cellular uptake of nanoparticles in these cells, we replaced ICG with FITC in the nanoparticles for the purpose of imaging. We were able to demonstrate in Figure 4A, that the CD44-negative MRC-5 cells were unable to internalize the HA-functionalized nanoparticles while CD44-positive H1299 and A549 cells were able to successfully internalize the HA-functionalized nanoparticles probably because of the presence of CD44 in the cell membrane. To confirm the involvement of CD44 in the uptake of HA-functionalized nanoparticles, cell line A549, H1299 AND MRC-5 were initially

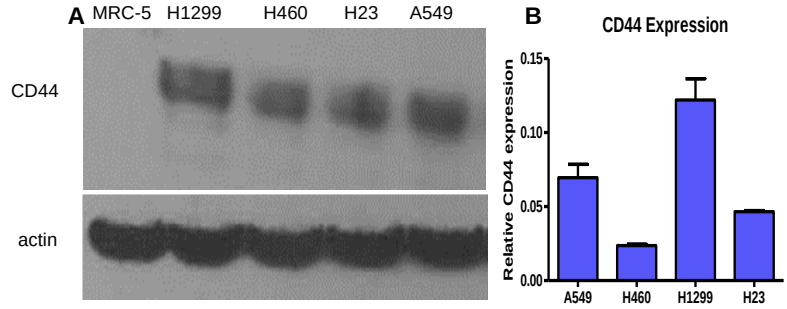

Figure 3. Expression of CD44 in some NSCLC cells. A. Western blot analysis of the expression of CD44 in some NSCLC cells in comparison to normal lung fibroblast MRC-5, B. RT-PCR analysis comparison the expression level of CD44 in some NSCLC cells

treated with free HA to inhibit CD44 before the cells were then treated with the nanoparticles. Corresponding cells that were not inhibited with free HA but treated only with HA-functionalized nanoparticles were also prepared. Cellular uptakes were quantified with flow cytometry. Figure 4B demonstrate that the uptake of nanoparticles by A549 and H1299 was significantly higher in the uninhibited cells in comparison to the HA-inhibited cells. Further, there was no significant difference in nanoparticle uptake between the inhibited and uninhibited MRC-5 cells.

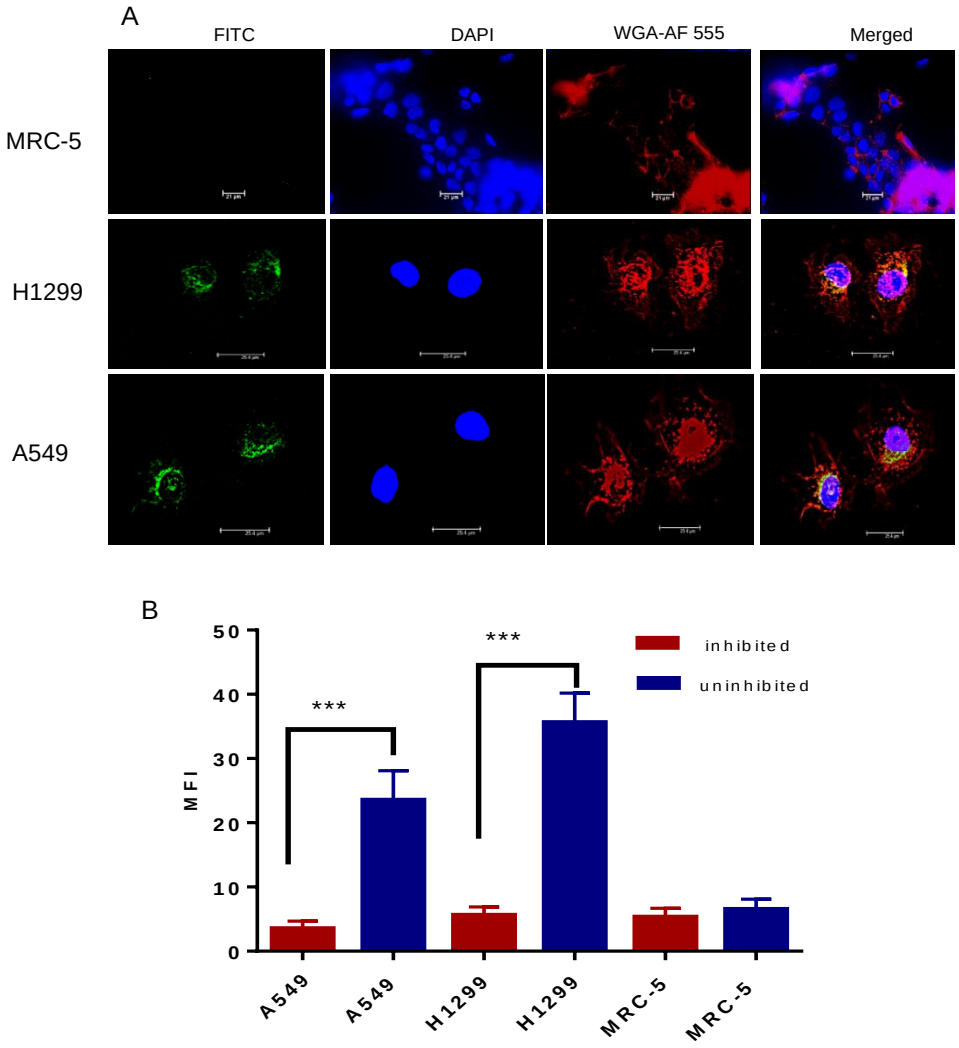

Figure 4. Intracellular trafficking of nanoparticles. A. Fluorescence micrograph. HA-functionalized-HSA-nanoparticles were loaded with FITC for intracellular monitoring. Internalized nanoparticles were imaged in different cells using fluorescence microscope. Top panel shows lack of internalizartion in MRC-5 cells. Middle panel shows efficient internalization in A549 cells. Lowest panel shows H1299 cells with very efficient nanoparticle uptake. B. Flow cytometry quantification of nanoparticle uptake in different cells after inhibition with free HA and uninhibited. ***P≤0.005. MFI – Mean Fluorescence Intensity

Cytotoxicity studies.

Anticancer effect of HA-functionalized-ICG-PTX-loaded nanoparticles was evaluated in A549 and H1299 cells in comparison to naked PTX and empty nanoparticles. As seen in Figure 5A, A549 cells' growth was inhibited by HA-functionalized-ICG-PTX-loaded nanoparticles in a superior manner in comparison to naked PTX. Similar trend was observed in H1299 cells in Figure 5B, suggesting that the encapsulation of PTX in the nanoparticles lead to an improved anticancer effect. Conversely, the empty nanoparticles did not show any antiproliferative effect suggesting that the empty nanoparticles were not toxic.

In vitro PA imaging

Performance of HA-functionalized-ICG-PTX-loaded nanoparticles as a potential contrast agent for PA imaging was evaluated in biological phantoms. Using blood vessel-mimicking tubes, we

evaluated the ability of these nanoparticles to enhance the signal sensitivity of ICG as compared to free ICG. Figure 7A demonstrates the superior PA average intensity (IPA) signal obtained from the HA-functionalized-ICG-PTX-loaded-nanoparticles in comparison to free ICG. While PBS (control) produced a IPA of 0.275, the free ICD sample produce an IPA of 1.275 while HA-functionalized-ICG-loaded nanoparticles produced an IPA of 2.609. Maximum PA intensities were obtained after laser irradiation at 806 nm. The PA signal seen in Figure 6A is an overlay with the ultrasound (US) signal from the tubes, which appears in grey. We calculated the IPA in selected regions of interest. To detect the signal of HA-functionalized-ICG-PTX-loaded nanoparticles at various depths, a chicken muscle phantom was used to mimic a tissue environment before imaging. This was done to ensure that PA imaging using ICG as a contrast agent could be applicable to orthotopic NSCLC mice models. Samples were injected at depths, 2, 5 and 10 mm into the chicken muscles. As can be seen, in Figure 6B, PA signals were detectable up to 10 mm in the muscle. This is very significant since the distance from the lung to the skin of a mice is approximately 9 mm [19]. The IPA signal from 2 mm is very low because a lot of the injected samples were lost to the top of the chicken phantom because of the shallow injection site. The ability of PA imaging to detect signal as deep as 10 mm is consistent with a previous report [20].The aqueous stability of free ICG was also compared to that of HA-functionalized-ICG-PTX-loaded nanoparticles using UV spectroscopy. Both samples were dispersed in PBS. As can be seen in Figure 6C, ICG loaded in the nanoparticles demonstrated superior stability over 48 hours in contrast to the free ICG that immediately showed decomposition within the first eight hours of incubation at 25°C. To have a clear idea of the impact of the nanoparticles on the stability of ICG, potential free ICG adsorbed on the surface of the nanoparticles were washed with the buffer before monitoring the stability of nanoparticle loaded ICG.

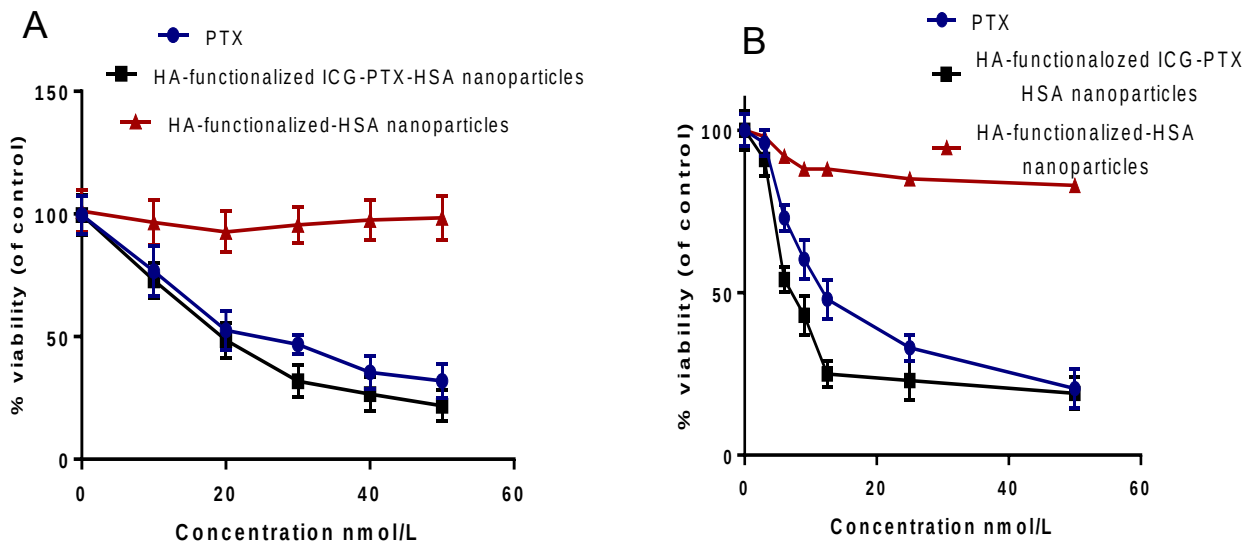

Figure 5. Anticancer activity studies. MTT assay was used to evaluate the ability of HA-functionalized ICG-PTX-loaded nanoparticles to inhibit the growth of two NSCLC cells in comparison to free PTX and empty nanoparticles. A. A549 cells and, B. H1299 cells.

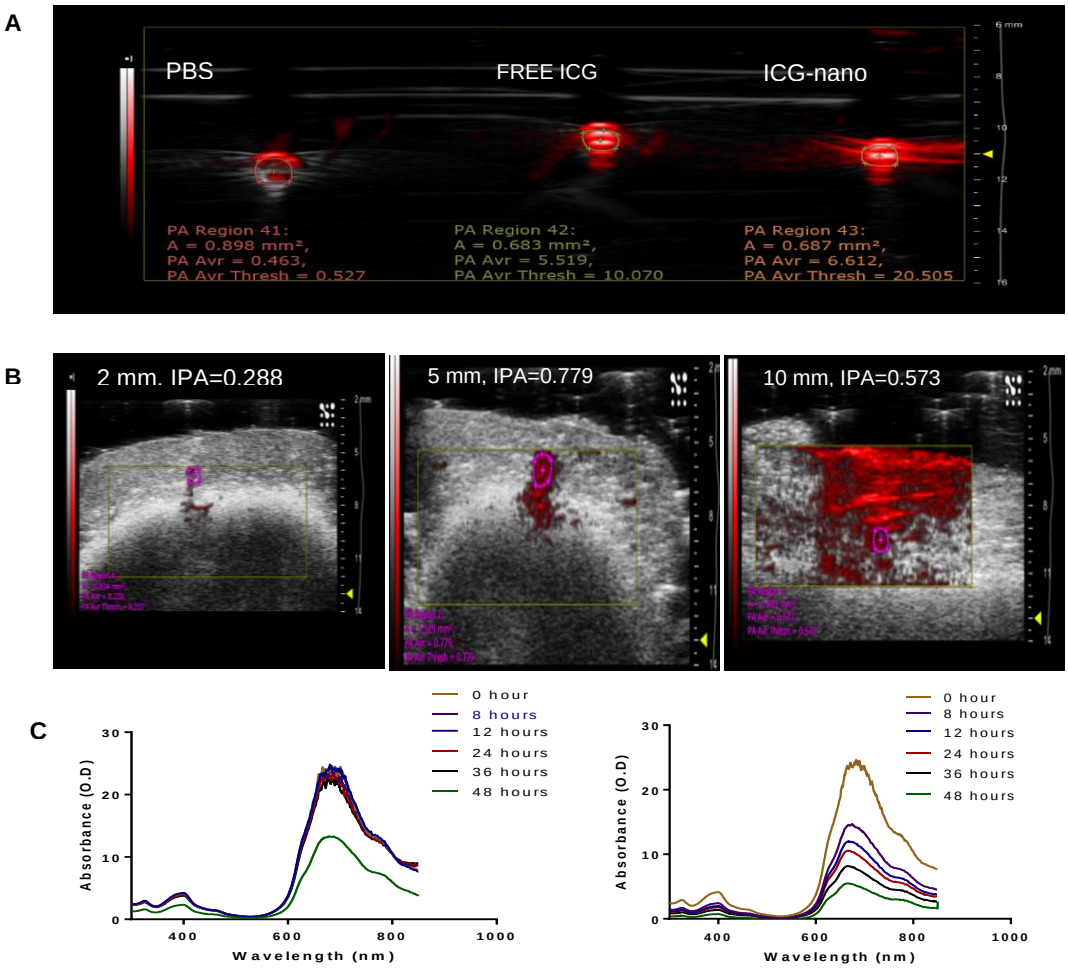

Figure 6. Photoacoustic imaging. A. Comparison of IPA signals between free ICG and HA-functionalized-ICG-loaded nanoparticles. B. Overlay of US and PA signals from HA-functionalized-ICG-PTX-loaded nanoparticles at different depths in chicken breast phantoms. C. Comparison of the aqueous stability of ICG in nanoparticles to free ICG in PBS.

Discussion

Chemotherapeutic agents such as PTX are often used in the treatment of NSCLC and other cancers. However, lack of selectivity in delivery to tumor tissues over normal tissues has been a challenging limitation to the continuous therapeutic use of chemotherapy. Nanoparticle delivery systems provide an opportunity to maximize the therapeutic use of chemotherapy in cancer. Through functionalization of nanoparticles with ligands that selectively target receptors/antigens on the surface of cancer cells, unwanted accumulation of nanoparticles in normal tissues/cells can be reduced. HA is a ligand that specifically binds to both standard and variant CD44 isoforms which are commonly expressed in lung cancer of the non-small cell type but not the small cell type [8]. Further, nanoparticles can be adapted for image-guided drug delivery to effectively manage cancer treatment by simultaneously treating and imaging of cancers. Such theranostic nanoparticles could provide a platform for image-guided therapy of cancers. An emerging area of biomedical science is the use of PA imaging as part of the tool for image-guided therapy, allowing the simultaneous imaging of the spread of cancer as well as the application of chemotherapy as needed. Recent studies have documented the use of PA to monitor the accumulation of nanoparticles in tumors [21, 22]. PA imaging combines high spatial resolution of ultrasound (US) and high contrast of optical imaging systems. Aside working at clinically relevant imaging depth, PA imaging enables the gathering of functional and molecular information in real time [9-10]. One of the most commonly used contrast agent for PA imaging is indocyanine green (ICG). ICG is a water soluble tricarbocyanine dye and along with methylene green, is the only dye, clinically approved near infrared red fluorophore. It has been approved by the FDA for human imaging and diagnosis in clinical applications [23]. However, ICG used in PA imaging is limited by its aqueous instability. It easily aggregates and undergoes irreversible degradation in aqueous medium leading to a very short biological half-life of 2-4 minutes [1]. In view of these limitations, there is an urgent need to formulate ICG in a way that can enhance its biological half-life and its selective delivery to diseased tissue in order to harness the advantages of PA imaging in disease diagnosis.

The overall objective of this study was to investigate the potential theranostic application of a nanoparticle delivery system composed of covalently bounded human serum albumin (HSA)-hyaluronic acid (HA) combination for efficient targeting of ICG and paclitaxel to lung tumor. We hypothesize that these nanoparticles will selectively and efficiently target CD44-positive NSCLC cells, facilitating its detection and improve its therapy by PA imaging.

HA was conjugated to the surface of the nanoparticles because it specifically binds to CD44. Both standard and variant CD44 isoforms are commonly expressed in lung cancer of the non-small cell type but not the small cell type [7]. It is rarely expressed in normal tissues, hence the decision to target it for selective targeting of NSCLC. HA-functionalized-ICG-PTX-loaded nanoparticles were prepared using HSA as the carrier resulting in nanoparticles of 315 nm slightly bigger is size than the non-functionalized nanoparticles. Conjugation of HA to ICG-PTX-loaded nanoparticles increase the size of the nanoparticles from 242.56 nm to 315.24 nm. The increase in size may be attributed to the conjugation of HA to the surface of the nanoparticles. Furthermore, the involvement of several centrifugation and lyophilization steps may also contribute to the increase in the particle size of the HA-functionalized nanoparticles [16]. Sonication of formulations before size measurement is a routine process. This is often done to make sure we are measuring single particles and not agglomerates. Often times, if sonication is not done we end up having false results leading to high PDI values.

The zeta potential (net charge) for all the nanoparticles were negative due to the fact that HSA is negatively charged in water at pH 7 [24]. The conjugation of HA to the ICG-PTX-loaded-HSA-nanoparticles led to more negatively charged nanoparticles because HA is a negatively charged polysaccharide, hence its presence on the surface of the HSA-nanoparticles further increased the negative charge of the nanoparticles [25]. Conjugation of HA to the HSA-nanoparticles was verified by FT-IR spectroscopy as shown in Figure 2C.

The release of both ICG and PTX from HA-functionalized ICG-PTX-loaded nanoparticles was monitored at pH values 7.4 and 6.6 to represent the pH values of the blood and tumor microenvironment, respectively [12]. Figure 2A shows that PTX demonstrated a more efficient release from the nanoparticles at pH 6.6 with approximately 100% of the drug released after 46 hr while only approximately 30% of PTX was released at pH 7.2. This suggests that the loaded PTX will not be released during circulation in the blood but rather in the tumor microenvironment. The reason for the more efficient release at pH 6.6 could be attributed to the acidic nature of the tumor microenvironment which facilitates the graduate erosion of the HSA-nanoparticles, hence enabling a slow but controlled release of the loaded PTX. Similar trend was observed for ICG in Figure 2B. However, ICG was released faster from the nanoparticles possibly because of its superior solubility in aqueous medium when compared to PTX, hence 100% loaded ICG was already release after 2 hr at pH 6.6 while only approximately 50% was released at pH 7.2.

The levels of CD44 expression in H460 and A549 cells as shown in Figure 3A are consistent with previous report by Penno et al. which showed that A549 had higher level of CD44 than H460 [26]. Our qRT-PCR results demonstrated that H1299 expressed the highest level of CD44 amongst all the cells studied. To elucidate the involvement of CD44 in the selective delivery of HA-functionalized ICG-PTX-loaded nanoparticles and to compare the uptake of HA-functionalized FITC-loaded nanoparticles in CD44+ cells to CD44- cells, MRC-5, A549 and H1299 cells were treated with these nanoparticles for 6 h. Fluorescence microscopy data in Figures 4 demonstrates that both A549 and H1299 NSCLC cells were able to internalize the FITC-loaded nanoparticles. On the other hand, MRC-5 cells did not internalize any visible FITC-loaded nanoparticles. We hypothesize that this was due to lack of CD44 on the surface of MRC-5 as demonstrated by data in Figure 3A. We were able to elucidate the involvement of CD44 in the preferential delivery of HA-functionalized ICG-PTX-loaded nanoparticles with this result.

The non-cytotoxicity of empty HA-functionalized-HSA nanoparticles was also demonstrated using MTT assay. However, While Plain PTX showed efficient anti-cancer activity in both A549 and H299 cells, a superior effect was demonstrated by HA-functionalized PTX-ICG-loaded nanoparticles.

To prepare HA-functionalized-ICG-PTX-loaded nanoparticles for application as a contrast agent in vivo, we tested these nanoparticles in biological phantoms. Using blood vessel-mimicking tubes, we evaluated the ability of these nanoparticles to enhance the signal sensitivity of ICG as compared to free ICG. Figure 6A demonstrates the superior PA average intensity (IPA) signal obtained from the HA-functionalized-ICG-loaded-nanoparticles in comparison to free ICG. While PBS (control) produced an IPA of 0.275, the free ICD sample produce an IPA of 1.275 while HA-functionalized-ICG-loaded nanoparticles produced an IPA of 2.609. Maximum PA intensities were obtained after laser irradiation at 806 nm. The PA signal seen in Figure 6A is an overlay with the ultrasound (US) signal from the tubes, which appears in grey. We calculated the IPA in selected regions of interest. To detect the signal of HA-functionalized-ICG-loaded nanoparticles at various depths, a chicken muscle phantom was used to mimic a tissue environment before imaging. This was done to ensure that PA imaging using ICG as a contrast agent could be applicable to orthotopic NSCLC mice models. Samples were injected at depths, 2, 5 and 10 mm into the chicken muscles. As can be seen, in Figure 6B, PA signals were detectable up to 10 mm in the muscle. This is very significant since the distance from the lung to the skin of a mice is approximately 9 mm [19]. The IPA signal from 2 mm is very low because a lot of the injected samples were lost to the top of the chicken phantom because of the shallow injection site. The ability of PA imaging to detect signal as deep as 10 mm is consistent with a previous report

[20].The aqueous stability of free ICG was also compared to that of HA-functionalized-ICG-loaded nanoparticles using UV spectroscopy. Both samples were dispersed in PBS. As can be seen in Figure 6C, ICG loaded in the nanoparticles demonstrated superior stability over 48 hours in contrast to the free ICG that immediately showed decomposition within the first eight hours of incubation at 25°C.

Conclusion

Molecular imaging using PA imaging is gradually gaining momentum, hence the development of an ideal nanoparticle delivery system is needed in tandem with this imaging technology. This current study has been able to show that PA imaging using ICG as part of image guided drug delivery could be enhanced by using HSA-based nanoparticle system that has been functionalized with HA to exploit the preferential expression of CD44 in NSCLC. HA-functionalized-ICG-PTX-loaded nanoparticles has potential for image-guided drug delivery in NSCLC treatment without compromising the anticancer efficacy of the loaded PTX.

References

1. Y-G. Wang, H. Kim, S. Mun, D. Kim, Y. Choi, Indocyanine green-loaded perfluorocarbon nanoparticles for bimodal ^{19}F-magnatic resonance/near infrared fluorescence imaging and subsequent phototherapy. Quant. Imaging Med. Surg. 3 (2003) 132-140
2. K. Y. Choi, G. Liu, S. Lee, X. Chen,Theranostic nanoplatforms for simultaneous cancer imaging and therapy: current approaches and future perspectives. Nanoscale 4 (2012) 330-342.
3. D. H. Kim, Image-guided cancer nanomedicine. J. Imaging. 4 (2018) 18.
4. F. Kratz, A clinical update of using albumin as a drug vehicle: A commentary. J. Control Rel. 190 (2014) 331-336.
5. E. Miele, G. P. Spinelli, E. Miele, F. Tamao, S. Tamao, Albumin-bound formulation of paclitaxel (Abraxane ABI-007) in the treatment of breast cancer. Int. J. Nanomedicine. 4 (2009) 99-105.
6. Y. Sheng, J. Xu, Y. You, F. Xu, Y. Chen. Acid sensitive peptide-conjugated doxorubicin mediates the lysosomal pathway of apoptosis and reverses resistance in breast cancer. Mol. Pharmaceutics. 12 (2015) 2217-2228.
7. G. Li, Y. Gao, Y. Cui, T. Zhang, R. Cui, Y. Jiang, J. Shi, Overexpression of CD44 is associated with the occurrence and migration of non-small cell lung cancer. Molecular Medicine Reports. 14 (2016) 3159-3167
8. E. L-H. Leung, R. R. Fiscus, J. W. Tung, V. R-C. Tin, L. C. Cheng, A. D-L. Sihoe, L. M. Fink, Y. Ma, M. P. Wong, Non small cell lung cancer cells expressing CD44 are enriched for stem cell like properties. Plos One. 5 (2010) e14062.
9. L. Wang, P. P. Yang, X. X. Zhao, H. Wang, Self assembled nanomaterials for photoacoustic imaging. Nanoscale. 8 (2016) 2488-2505.
10. M. L. James, S. S. Gamshir, A molecular imaging primer: modalities, imaging agents and applications. Physiol. Rev. 92 (2012) 897-965.
11. Hou D, Gui R, Hu S. et al. (2015). Preparation and characterization of novel drug-inserted montmorillonite chitosan carriers for ocular drug delivery.. Adv. In Nanoparticles. 4, 70-84.
12. Perepelyuk, M, Maher, C, Lakshmikuttyamma, A, Shoyele, S. A. (2016). Aptamer-hybrid Nanoparticle Bioconjugate Efficiently Delivers miRNA-29b to Non-Small cell Lung Cancer Cells and Inhibits Growth by Downregulating Essential Oncoproteins. Int. J. Nanomedicine. 11, 3533–3544.
13. C. Ruckman, S. Z. Shaikh, P. Khalil, M. S. Muneera, O. A. Thusleem, Determination of sodium hyaluronate in pharmaceutical formulations by HPLC-UV. J. Pharm. Anal. 3 (2013) 324-329.
14. I. Badea, D. Ciutaru, L. Lazar, D. Nicolescu, A. Tudose, Rapid HPLC method for the determination of paclitaxel in pharmaceutical forms without separation. J. Pharmaceut. Biomed. 34 (2004) 501-507.
15. Y. Sheng, J. Xu, Y. You, F. Xu, Y. Chen. (2015). Acid sensitive peptide-conjugated doxorubicin mediates the lysosomal pathway of apoptosis and reverses resistance in breast cancer. Mol. Pharmaceutics. 12, 2217-2228
16. A. Srinivasan, S. A. Shoyele. Influence of surface modification and pH on the release mechanisms and kinetics of erlotinib from anti-body functionalized chitosan nanoparticles. Ind. Eng. Chem. Res. 53 (2014) 2987-2993
17. M. Guo, P. Diao, S. Cai, Hydrothermal growth of well aligned ZnO nanorod arrays: dependence of morphology and alignment ordering upon preparing conditions J. Solid State Chem. 178 (2005) 1864-1873.

18. M. AbdElhady, Preparation and characterization of chitosan/zinc oxide nanoparticles for imparting antimicrobial and UV protection to cotton fabric. Int. J. Carbohydr. Chem. (2012). Article ID 840591.
19. G. H. Im, M-S. Jang, J. J. Chung, K-N. Kim, J-H. Kim, S. I. Kim, J. H. Lee, Improvement of orthotopic lung cancer mouse model via thoracotomy and orotraccheal intubation enabling in vivo imaging studies. Laboratory Animals. 48 (2014) 124-131.
20. N. Beztsinna, Y. Tsvetkova, J. Jose, B. Rhourri-Frih, W. Al Rawashdeh, T. Lammers, F. Kiessling, L. Bestel Photoacoustic imaging of tumor targeting with riboflavin-functionalized theranostic nanocarriers Int. J. Nanomedicine. 12 (2017) 3813-3825.
21. L. Wang, P. P. Yang, X. X. Zhao, H. Wang, Self-associated nanomaterials for photoacoustic imaging. Nanoscale. 8 (2016) 2488-2509.
22. G. P.Luke, D. Yeager,S. Y. Emelianov, Biomedical application of photoacoustic imaging with exogenous contrast agents. Ann. Biomed. Eng. 40 (2012) 422-437.
23. K. E, Wilson, T. Y. Wang, J. K. Willmann, Acoustic and photoacoustic molecular imaging of cancer. J. Nucl. Med. 54 (2013) 1851-1854
24. K. Baler, O. Martin, M. A. Carigno, G. A. Ameer, J. A. Vila, I. Szleifer, Electrostatic unfolding and interactions of albumin driven by pH changes: A molecular dynamic study. J. Phys. Chem. B. 118 (2004) 921-930.
25. F. Horkay, P. J. Basser, D. J. London, A.M. Hecht, E. Geissler, Ions in hyaluronic acid solutions. J. Chem. Phys. 131 (2009) 184902.
26. M. B. Penn, J. T. August, S. B. Baylon, M. Mabry, R. I. Linnoila, V. S. Lee, Expression of CD 44 in human lung tumors. Cancer Res. 54 (1994) 1381-1387.